Implementation of Radiation and Soil Losses in VFTO Simulation by Frequency-Domain TL Model

Jun Zhao, Weijiang Chen, *Senior Member, IEEE*, Kejie Li, Kai Bian, Jiangong Zhang, Tao Wen, and Zihan Teng

***Abstract*—Transmission line (TL) models are widely used within the simulation of the very fast transient over-voltages (VFTO) for gas-insulated substations (GISs); however, due to quasi-TEM approximation and model complexity, energy losses related to bushing radiation and frequency-dependent soil parameters are either not available or simply neglected, limiting the simulation accuracy of TL models. In this study, a new frequency-domain TL model is proposed, enabling the model to consider the influences of both radiation and soil losses in a VFTO simulation. Derived from the radiation power of a line antenna model, the radiation resistance of a "lossy" TL is put forward as an equivalent of the radiation loss for GIS bushing. For the soil loss, the Sunde approximation formula and the L-S soil dispersion expression are involved, and the parameters of the overhead busbar are also analyzed. The model gets validation by the measured VFTO generated at a full-scale 1100 kV GIS testing circuit. By considering radiation loss to suppress high-frequency response and soil loss to improve low-frequency response accuracy, the calculated and measured waveforms have the best consistency, which may greatly help assess the risk of insulation breakdown and the level of very fast transient disturbance in GISs.**

***Index Terms*—VFTO, radiation loss, soil loss, electromagnetic transient simulation.**

I. Introduction

Very fast transient over-voltages (VFTO) are generated during switching operations of gas-insulated substation (GIS) disconnectors because of voltage collapse across the inter-contact gap at striking and traveling waves propagating along the pipeline [1]. Typically, the rise time of the VFTO front is several nanoseconds, substantially lower than the transmission time of the associated traveling waves passing through the GIS components. This causes the traveling waves that propagate back and forth to reflect at any surge impedance discontinuity, eventually superimposing to constitute the VFTO in the GIS [2]–[4].

The VFTO simulation is significant for supporting the GIS insulation design, particularly with the voltage classes of extra-high voltage (EHV) and ultra-high voltage (UHV), as the insulation withstand voltage levels are lower compared to that defined for lower rated voltages [5]. During the commissioning of UHV substations in China, there have been some GIS pipeline breakdown events caused by VFTOs, and the specific reasons for the risks are still unclear. Moreover, due to the increasing applications of on-site electronic devices at GIS substations in recent years, the transient disturbances originating from the VFTO might cause severe failures on these on-site devices [6], [7], making the VFTO simulation also important for electromagnetic compatibility design.

The predominantly used approach is based on solving equations for lumped circuit models and transmission line (TL) models that represent GIS components [8], with the use of any transient simulation software (e.g., ATP - EMTP [9]) in the time-domain algorithm. However, compared to the measured VFTO waveform generated on our UHV AC Test Base, it can be found that the calculated waveform has more high-frequency "glitches" and is prone to misestimate the main low-frequency oscillations of hundreds of kilohertz [10]. The inaccuracy in the VFTO calculation indicates that the energy losses in the corresponding frequencies are not accurately considered in GIS component models.

There exist arc loss, skin loss, radiation loss, and soil loss in the very fast transient (VFT) due to the switching operation of the disconnectors [11]. The arc loss is typically represented using time-varying resistances such as the exponential resistance [12], segment resistance [13], and nonlinear resistance defined by the Toepler formula [14]. For the skin loss of a busbar, it can be easily expressed as the skin impedance with the form of $\mathrm{A} + \mathrm{B}\sqrt{\mathrm{s}}$ through the Laplace equation, which can be applied to the time-domain algorithm [15]. However, unlike arc loss and skin loss, radiation loss and soil loss have not been well considered in existing models. The existing TL model of GIS bushing ignores the radiation loss, which is caused by electromagnetic leakage because the bushing shield is discontinuous. Soil loss is also ignored or simplified in time-domain algorithms because of the complex frequency-dependent characteristics of the earth parameter. In addition, the soil has a dispersion effect, i.e., the

---

Manuscript received 19 December 2021; revised 31 March 2022; accepted 9 May 2022. Date of publication 3 June 2022; date of current version 28 November 2022. This work was supported by the National Natural Science Foundation of China under Grant 51977199. Paper no. TPWRD-01894-2021. *(Corresponding author: Kejie Li.)*

Jun Zhao, Jiangong Zhang, and Zihan Teng are with the High Voltage Branch, China Electric Power Research Institute, Wuhan 430074, China (e-mail: 278850774@qq.com; zhangjiangong@epri.sgcc.com.cn; 862269519@qq.com).

Weijiang Chen and Kai Bian are with the State Grid Corporation of China, Beijing 100031, China (e-mail: weijiang-chen@sgcc.com.cn; kai-bian@sgcc.com.cn).

Kejie Li and Tao Wen are with the School of Electrical Engineering and Automation, Hefei University of Technology, Hefei 230009, China (e-mail: kejie.li@hotmail.com; tao-wen@xjtu.edu.cn).

Color versions of one or more figures in this article are available at https://doi.org/10.1109/TPWRD.2022.3177766.

Digital Object Identifier 10.1109/TPWRD.2022.3177766

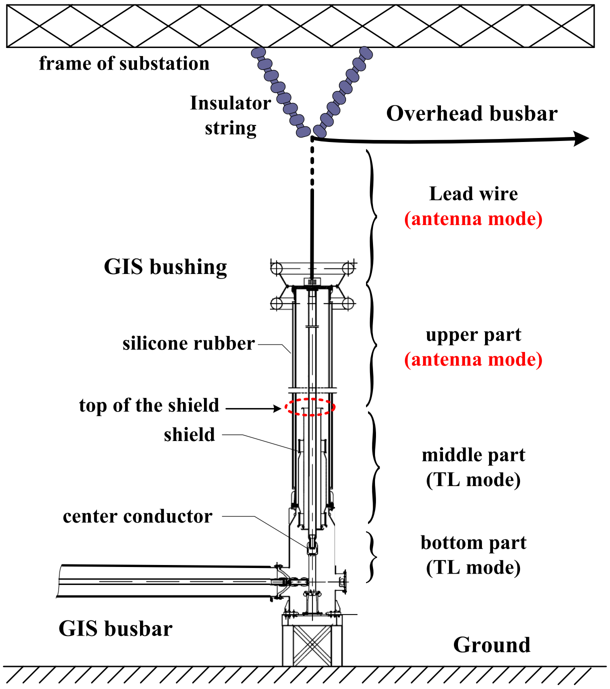

Fig. 1. Structure of GIS bushing divided by the bottom and middle parts in the TL mode and the upper part and lead wire in the antenna mode.

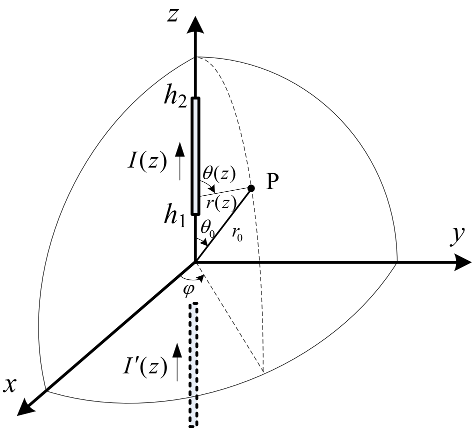

Fig. 2. Schematic of a spherical coordinate system for radiation fields calculation.

conductivity and permittivity are frequency dependent, which has been valued in lightning transient simulations [16]–[19]; however, its role in VFTO simulations remains unclear.

In this paper, we present models of radiation and soil losses in a VFTO simulation to improve the simulation accuracy covering a wider spectrum. First, we analyze the current distribution at the GIS bushing, deduce the radiated electromagnetic field and its power loss, and then propose a new TL model with radiation resistance for the bushing considering the radiation loss. Second, we analyze the influence of soil dispersion on the earth impedance of the TL model of the overhead busbar, and analyze the contribution of each parameter of the TL model and propose a simplification in simulation. Subsequently, we propose a VFTO frequency domain algorithm and the excitation source settings to facilitate the processing of frequency-dependent parameters related to the radiation and soil losses. Finally, by comparing the measured and calculated waveforms of the VFTO in a full-scale 1100 kV GIS test circuit, the significance of considering the radiation and soil losses for the VFTO simulation is analyzed.

II. GIS Bushing Modeling With Radiation Loss

A. *Analysis of the Current Distribution*

The GIS bushing consists of a center conductor, a shield and a silicone rubber shell for connecting the GIS pipeline to the overhead busbar (Fig. 1). When the VFT travels to the bushing, the conductor and metal enclosure at the bottom part form a transmission line, the conductor and metal shield in the middle part also form a transmission line, while the upper part and the lead wire form an antenna, radiating the electromagnetic field and causing the radiation loss, which is non-TEM [20].

Since the excitation of the antenna mode part of the bushing is unknown in advance, the method of moments cannot be used to accurately calculate the current distribution, and the characteristic impedance analysis method is more suitable.

The characteristic impedance of each part of the vertical bushing conductor can be expressed by [21]:

$$Z_c = \frac{\sqrt{\mu_0/\varepsilon_0}}{2\pi} \ln \frac{2h}{m} = 60 \ln \frac{2h}{m} \tag{1}$$

where *h, m* are the height and radius of the conductor respectively, and μ_0, ε_0 are the vacuum permeability and permittivity, respectively.

The characteristic impedance along the line of the bushing antenna mode is found to change very slowly. For UHV bushings, the characteristic impedance slowly rises from 310.8 Ω at the shield opening to 376.7 Ω at the top of the lead wire, and the traveling wave reflectivity along the line gradually decreases from 1.20% to 0.33%, and the total reflectivity is less than 10%. The reflectivity is so small that the attenuation of the TL current along the bushing can be ignored, which is different from the current distribution along the lightning channel. Thus the current distribution can be expressed as:

$$I(z) = I_0 e^{-jkz} \tag{2}$$

where I_0 is the current amplitude, $k = \omega/v$ is the phase shift constant in which ω is the angular frequency and *v* is the wave speed, and *z* is the position.

B. *Calculation of Radiation Resistor*

Now the loss from antenna mode is derived. Considering the equivalent line antenna composed by the upper part, the lead wire, and their images under the ground (Fig. 2), the far field components can be expressed by:

$$E_\theta = \frac{jkZ_0}{4\pi}\left(\int_{h_1}^{h_2}\frac{I(z)sin\theta(z)e^{-jkr(z)}}{r(z)}dz + \int_{-h_2}^{-h_1}\frac{I(z)sin\theta(z)e^{-jkr(z)}}{r(z)}dz\right) \quad (3)$$
$$H_\varphi = E_\theta / Z_0$$

where Z_0 is the spatial wave impedance, $r(z)$ is the distance of the observation point from the current element, and dz is the length of the current element.

Both the angleθ and the distance r vary with the position z. In the far field, the following approximations can be made:

$$r(z) \approx r_0 \quad (4)$$

$$\sin\theta(z) \approx sin\theta_0 \quad (5)$$

$$e^{-jkr(z)} \approx e^{-jkr_0}e^{jkz\cos\theta_0} \quad (6)$$

where r_0 and θ_0 are the distance and angle of the observation point from the origin, respectively.

To facilitate the calculation of radiation power, the electric and magnetic fields can ignore the same phase factor e^{-jkr_0}, and their expressions are simplified to:

$$E_\theta = \frac{jkZ_0 I_0 \sin\theta_0}{4\pi r_0}\left(\int_{h_1}^{h_2} e^{-jkz}e^{jkz\cos\theta_0}dz + \int_{-h_2}^{-h_1} e^{-jkz}e^{jkz\cos\theta_0}dz\right) \quad (7)$$

$$H_\varphi = \frac{jkI_0\sin\theta_0}{4\pi r_0}\left(\int_{h_1}^{h_2} e^{-jkz}e^{jkz\cos\theta_0}dz + \int_{-h_2}^{-h_1} e^{-jkz}e^{jkz\cos\theta_0}dz\right) \quad (8)$$

where h_1 and h_2 are the heights of the two ends of the conductor from the ground.

The radiation power is the integral of the average power flow density in the half sphere above the ground.

$$P = \int_S S_{avg}\cdot dS = \int_0^{\pi/2}\int_0^{2\pi}\frac{1}{2}\mathrm{Re}(E\times H^*)\cdot\hat{r}r_0^2\sin\theta_0 d\theta_0 d\varphi \quad (9)$$

Therefore, the formula for the radiation resistance of the bushing is derived as follows:

$$R_\mathrm{d} = \int_0^{\pi/2}\frac{\sin^3\theta_0\{\sin kh_2(cos\theta_0 - 1) - sinkh_1(cos\theta_0 - 1)\}^2}{2\pi(cos\theta_0 - 1)^2/Z_0}d\theta_0 \quad (10)$$

C. Lossy TL Modeling of GIS Bushing

Since the attenuation of TL current is negligible due to the small reflectivity, the radiation loss becomes the main factor decreasing the current up-forward, which makes the attenuated current distribution along the vertical conductor above ground non-TEM. In order to build a TEM model as well, a “lossy” TL with resistor in series is proposed, by which the radiation loss can be represented as the resistance along the line (see Fig. 3).

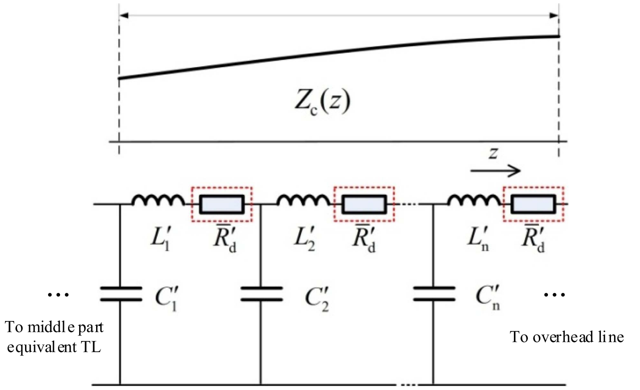

Fig. 3. Improved GIS bushing model with equivalent average radiation resistance $\bar{R}'_\mathrm{d}$ to consider the radiation loss, as the characteristic impedance $\mathrm{Z_c}(z)$ along the vertical conductor changes gradually.

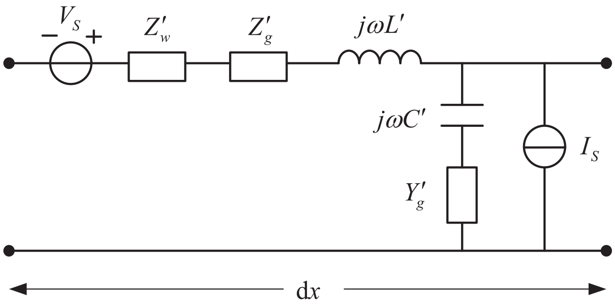

Fig. 4. Per-unit-length circuit of the TL model of the overhead busbar.

The radiation resistance per unit length can be approximately calculated as an average of the total radiation resistance along the whole line. Thus, the radiation loss can be easily solved by classic TL model, without adding new type of circuit model or introduce a full-wave simulation.

III. Overhead Busbar Modeling With Soil Loss

A. Lossy TL Modeling of GIS Bushing

The overhead busbar is commonly modeled as a transmission line in the VFTO simulation (Fig. 4), although some high-frequency components don’t strictly follow the quasi-TEM mode for the TL assumption [22]–[24].

The longitudinal impedance and transversal admittance of the overhead busbar are shown as follows [25]:

$$Z'(\omega) = j\omega L' + Z'_g + Z'_w \quad (11)$$

$$Y'(\omega) = (1/j\omega C' + 1/Y'_g)^{-1} \quad (12)$$

where L', Z'_g and Z'_w are the external inductance, earth impedance and internal impedance, respectively; C' is the capacitance and Y'_g is the earth admittance.

B. Influence of Soil Dispersion

The earth impedance and earth admittance can be calculated by Sunde expression [26], [27]:

$$Z_g' = \frac{j\omega\mu_0}{2\pi}\ln\frac{1+\gamma_g h}{\gamma_g h} \tag{13}$$

$$Y_g' \approx \gamma_g^2 / Z_g' \tag{14}$$

where μ_0 ,ε_0 are the vacuum permeability and permittivity, respectively; $\gamma_g = \sqrt{j\omega\mu_0(\sigma_g + j\omega\varepsilon_g\varepsilon_0)}$ is the propagation constant in the soil, with $\omega = 2\pi f$ the angular frequency, σ_g and ε_g the conductivity and relative permittivity of the soil, respectively.

As the frequency of the external electric field increases, the increase in soil polarization loss leads to an increase in the effective conductivity and a decrease in the permittivity, which is called the dispersion effect of soil. Compared with the soil dispersion models such as Portela, Visacro-Alipio, the Longmire-Smith model is employed in the earth impedance and admittance calculations because of its suitable bandwidth of 100 Hz-200 MHz [28].

$$\varepsilon_{\mathrm{g}}(f) = \varepsilon_\infty + \sum_{i=1}^{13} a_i\left[1+\left(\frac{f}{F_i}\right)^2\right]^{-1} \tag{15}$$

$$\sigma_{\mathrm{g}}(f) = \sigma_0 + 2\pi\varepsilon_0\sum_{i=1}^{13} a_i F_i\left(\frac{f}{F_i}\right)^2\left[1+\left(\frac{f}{F_i}\right)^2\right]^{-1} \tag{16}$$

where $\varepsilon_\infty' = 5$ is the asymptotic value of the relative permittivity; σ_0 is the low-frequency soil conductivity; f is frequency; a_i and F_i are the coefficients given in [29].

Fig. 5 takes the UHV overhead busbar as an example to analyze the influence of soil dispersion on earth impedance. Whether the dispersion is considered or not, the real part decreases as the soil conductivity increases, and increases as the frequency increases. The dispersion works in the frequencies above megahertz where the real part will decrease, a phenomenon that is more pronounced with smaller soil conductivity. The variation of the imaginary part with frequency is quite different due to it no longer increases monotonously but has an extreme point for the soil conductivity of 0.01 S/m and 0.001 S/m. In most cases, dispersion will also reduce the imaginary part.

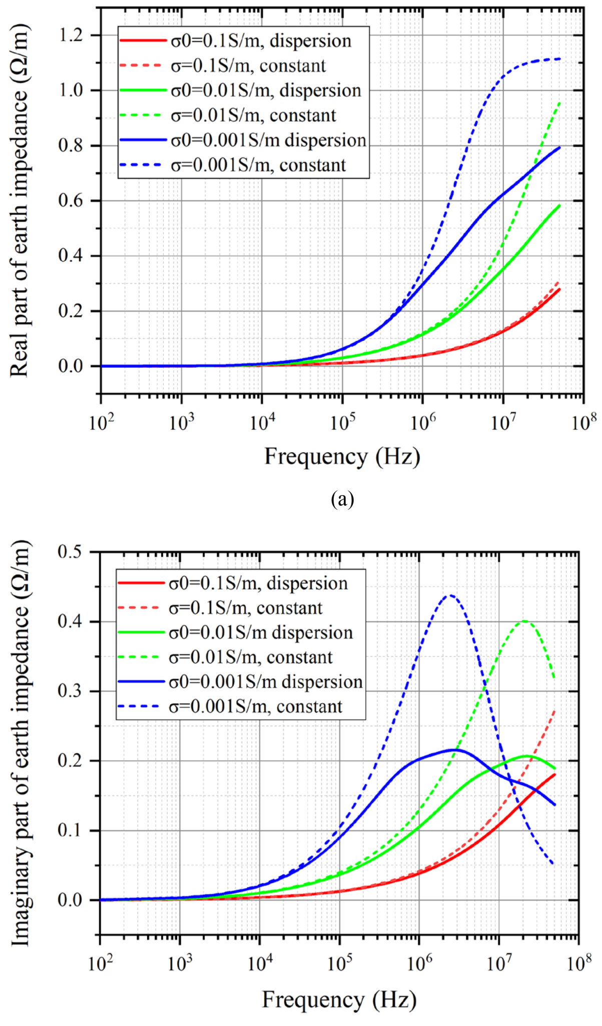

(a)

(b)

Fig. 5. Comparisons of earth impedance with and without considering dispersion for UHV overhead busbar in Wuhan Test Base. The center height of the busbar is 24 m. The low-frequency conductivity is taken as 0.1, 0.01, and 0.001 S/m to cover the common range. (a) Real part; (b) Imaginary part.

C. Analysis of TL Parameters

TL parameter analysis can explain the main source of loss and verify the rationality of ignoring earth admittance, so as to explore the possibility of model simplification.

The internal impedance of the overhead busbar can be calculated by the Nahman and Holt equation [30]. For multi-split conductors, the result needs to be divided by the number of splits.

$$Z_w' \approx \left(\frac{1}{\pi a^2\sigma_w} + \frac{1}{2\pi a}\sqrt{\frac{\mu_w}{\sigma_w}}\sqrt{\mathrm{j}\omega}\right) \tag{17}$$

where σ_w is the conductivity of conductor; μ_w is the permeability of conductor; a is the radius of conductor.

The inductance and capacitance of a multi-split conductor can be calculated by using the equivalent radius and center height.

$$L' = \frac{\mu_0}{2\pi}\ln\frac{2h}{r_{eq}}, C' = \frac{1}{2\pi\varepsilon_0}\ln\frac{2h}{r_{eq}} \tag{18}$$

where h is the center height of the multi-split conductor; $r_{eq} = \sqrt[n]{r\prod_{k=2}^{n} d_{1k}}$ is equivalent radius, with d_{1k} the distance between the first and the k sub conductors, and $\prod$ the symbol of multiplication.

Fig. 6 shows the results of the TL parameter analysis of the UHV overhead busbar considering the soil dispersion effect and the soil conductivity range. Among the longitudinal impedance parameters, the external inductance contributes most of the inductance component, and the earth impedance far exceeds the internal impedance, indicating that the soil loss far exceeds the conductor skin loss. The admittance of an overhead busbar is

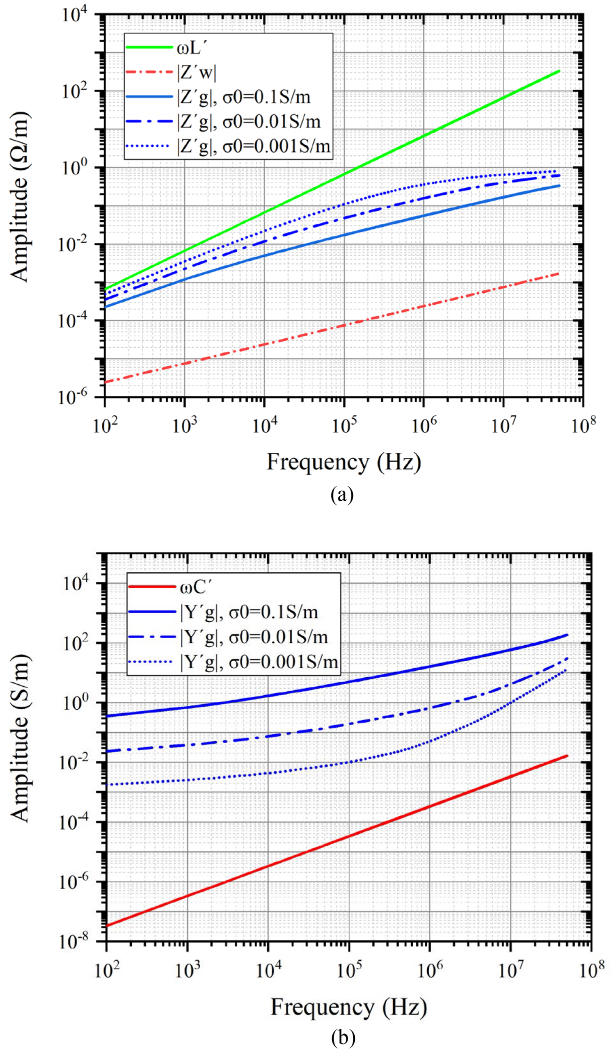

Fig. 6. Comparisons of TL parameters with frequency for UHV overhead busbar in Wuhan Test Base. The busbar is 4-split conductor, with the radius of 2.764 cm and the adjacent distance of 45 cm. (a) Longitudinal impedance parameters; (b) Transversal admittance parameters.

composed of two parts: the capacitance of the overhead conductor relative to the ground, and the capacitance and conductance in the earth admittance. The earth admittance varies with frequency and soil parameters. However, for the case of the overhead busbar, the earth admittance can be ignored as its influence on the total shunt admittance is negligible, according to (12).

From the propagation constant, it is more convenient to see that the loss of the overhead busbar mainly comes from the earth impedance, more specifically corresponding to the actual part, as

$$\gamma = \sqrt{Z'(\omega)Y'(\omega)} \approx \sqrt{\frac{j\omega L' + Z'_g}{1/j\omega C' + 1/Y'_g}} \approx \sqrt{(j\omega L' + Z'_g)j\omega C'} \quad (19)$$

This also means that the capacitance of the overhead conductor relative to the ground is so small that the loss caused by the displacement current can be ignored. This inference is consistent with the conclusion pointed out in [31] that the earth admittance needs to be considered only when the wire is at or under the ground. In short, the internal impedance of conductor and the earth admittance in the overhead busbar model can be ignored in VFTO simulations.

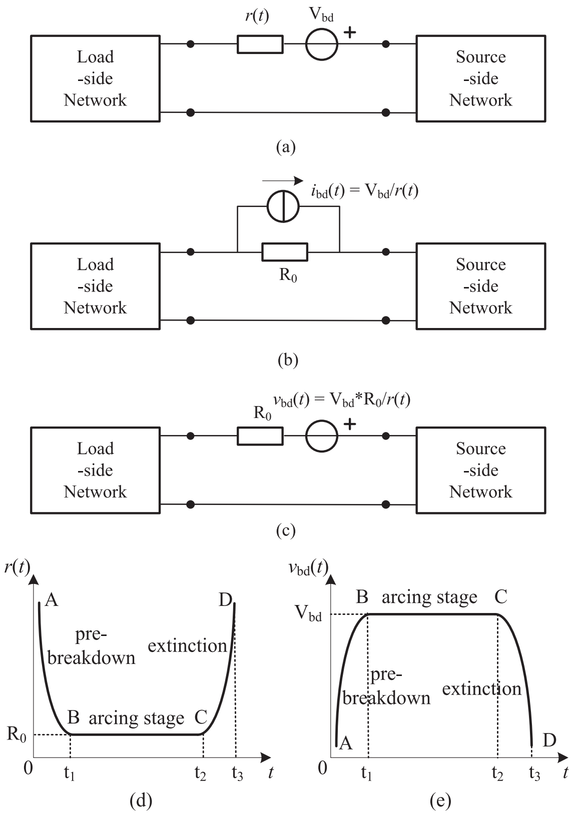

Fig. 7. Equivalent adjustment process of the excitation circuit. (a) Normally used excitation circuit in the time-domain simulation. (b) Excitation circuit with time-varying current source by Norton equivalent. (c) Excitation circuit with the time-varying voltage source by Thevenin equivalent. (d) Waveform of time-varying arc resistance. (e) Waveform of time-varying voltage source.

IV. VFTO FREQUENCY-DOMAIN ALGORITHM

To deal with the complex frequency-dependent parameters such as the radiation resistance and the earth impedance, an algorithm in the frequency domain is proposed for VFTO simulation. Some strategy is adopted on the arc excitation source so that the requirements of linear superposition for the Fourier transform can be facilitated.

Fig. 7 shows the three-step adjustment process how the time-varying resistance $r(t)$ is handled. Firstly, the Norton equivalent is used to get the time-varying current source $i_{\rm bd}(t) = {\rm V_{bd}}/r(t)$; however, it can be simplified as a static resistance $\rm R_0$ given that the arc loss occurs during the stable arcing stage. Secondly, the Thevenin equivalent is used to get the time-varying voltage source $v_{\rm bd}(t) = {\rm V_{bd}}{*}{\rm R_0}/r(t)$ with the series resistance $\rm R_0$. Since the $r(t)$ is within the excitation now, there is no time-varying item in the transfer function of the system itself. Finally, the Fourier transform can be performed on the time-varying voltage source

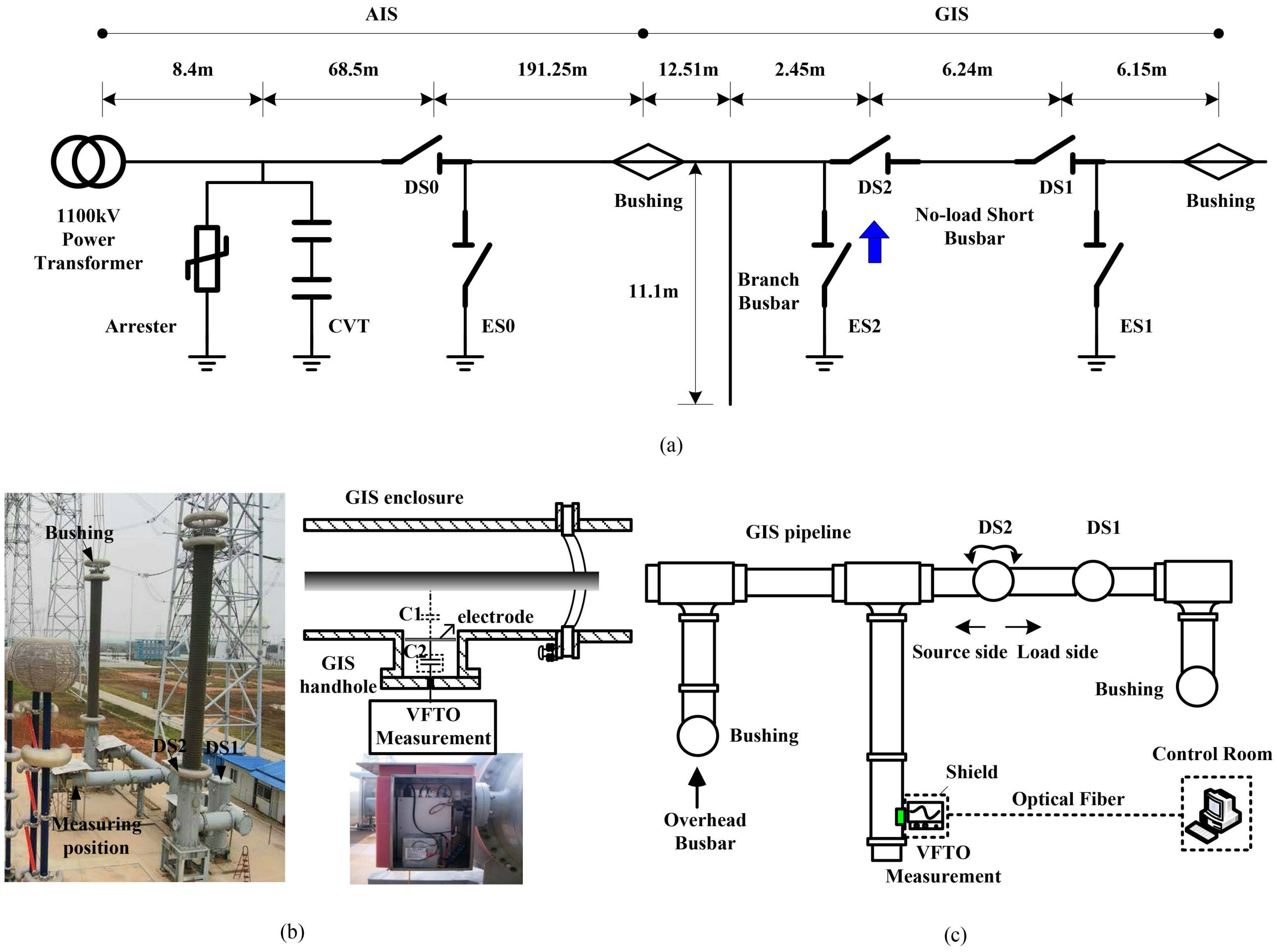

(a)

(b)

(c)

Fig. 8. Full-scale 1100 kV GIS test setup in the UHV Test Base. (a) Panoramic images of the test circuit. (b) Schematic and image of VFTO measurement. (c) Schematic of GIS disconnector switching operation.

to obtain the excitation in the frequency domain. Moreover, since the pre-breakdown is only a few nanoseconds, and the arc extinguishing occurs after the VFTO, the two have little effect on the transient analysis and can be ignored. Therefore, the equivalent excitation source can be further transformed into an ideal step pulse.

Thus, the VFTO time-domain waveform can be obtained by the inverse Fourier transform of the spectral response:

$$\begin{aligned} v(t) &= \frac{1}{2\pi}\int_{-\infty}^{+\infty} F(\omega)G(\omega)e^{j\omega t}d\omega \\ &= \frac{1}{2\pi}\sum_{0}^{n_0}\frac{1}{jn\Delta\omega}G(n\Delta\omega)e^{jn\Delta\omega t}\Delta\omega \\ &\quad + \frac{1}{2\pi}\sum_{0}^{n_0}\text{conj}[\frac{1}{jn\Delta\omega}G(n\Delta\omega)]e^{-jn\Delta\omega t}\Delta\omega \end{aligned} \tag{20}$$

where $F(\omega)= 1/(\mathrm{j}\omega)+\pi\delta(\omega)$ is the spectrum of step excitation voltage, in which $\pi\delta(\omega)$ can be ignored due to zero system response for the DC component; $G(\omega)$ is the system response of the TL network;$\Delta\omega$ is the sampling interval, n_0 is the number of samples, and $n_0\Delta\omega= 50\text{MHz}$. The error mainly comes from $e^{jn\Delta\omega t}$, thus the smaller the $\Delta\omega$, the higher the calculation accuracy.

V. MODEL EXPERIMENTAL VALIDATION

A. *Full-Scale 1100 kV GIS Test Setup*

The full-scale 1100 kV GIS circuit in the UHV AC Test Base is used to verify the proposed models. Fig. 8 shows the test circuit setup and VFTO measurement arrangement. The GIS part consists of GIS busbars, two GIS bushings, two GIS disconnectors (DS1 and DS2) and two earthing switches (ES1 and ES2). The GIS bushing at the left side is connected to a power transformer through an overhead busbar, along which an arrester, a capacitive voltage transformer (CVT), an AIS disconnector (DS0) and an earthing switch (ES0) are installed. During the test, the power transformer energizes the GIS circuit through the overhead busbar, and DS1 remains in the open state, and DS2 is initially open and then is closed to generate the VFTO. The signal is measured by a hand-hole sensor with a bandwidth of 0.3 Hz–300 MHz [32], and then transmitted to the computer in the control room through the optical fiber.

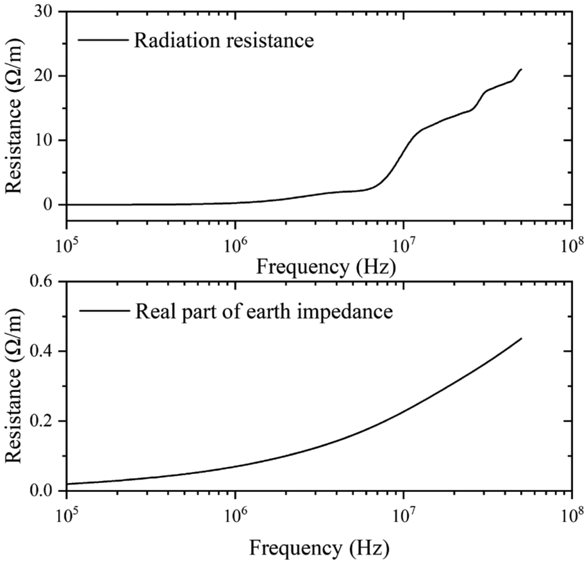

Fig. 9. Per-unit-length radiation resistance of the UHV GIS bushing and real part of the earth impedance of the UHV overhead busbar.

TABLE I
EQUIVALENT CIRCUITS OF OTHER COMPONENTS IN THE TEST CIRCUIT

Components	Equivalent circuits	Description
GIS busbar	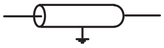	TL model with a characteristic impedance of 95 Ω
Overhead busbar	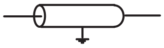	TL model with a characteristic impedance of 303 Ω ~ 372 Ω
GIS bushing in TL mode	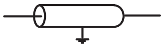	TL model with a characteristic impedance of 47 Ω for middle part and 107 Ω for bottom part
Basin insulator	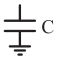	Lumped capacitance of 10 pF
GIS Disconnector DS1 in open state	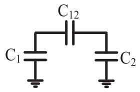	Lumped capacitance of 20 pF between the fractures and 10 pF for the electrodes to ground
AIS Disconnector DS0 in closed state	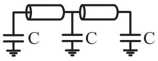	TL with a characteristic impedance of 304 Ω, and lumped capacitance of 150 pF for the electrodes to ground
CVT	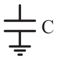	Lumped capacitance of 5000 pF
Arrester	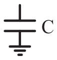	Lumped capacitance of 20 pF
Power transformer	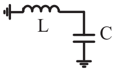	Lumped capacitance of 3000 pF, and lumped inductance of 10 mH

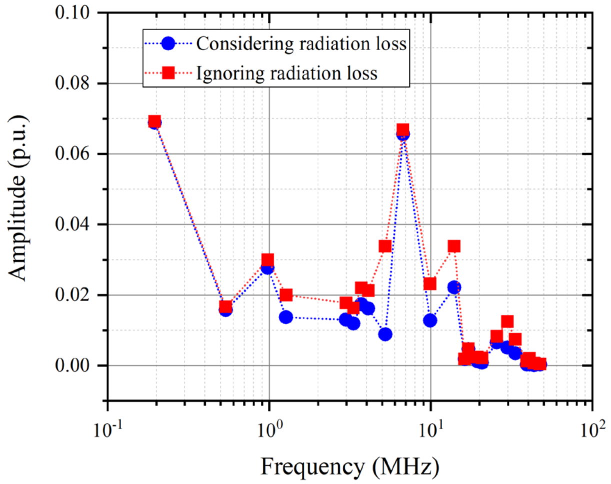

Fig. 10. Comparison between the amplitude–frequency responses of VFTO considering the radiation loss and ignoring the radiation loss. The breakdown voltage used for calculation is 1 p.u.

For such a test setup of the 1100 kV GIS circuit, the high-frequency component of the VFTO should come from the resonance of the GIS busbar and the low-frequency component of the VFTO from the resonance of the overhead busbar connecting the GIS and the power transformer [33].

B. Models of the Components in GIS Circuit

The proposed GIS bushing model is used to consider the radiation loss. The radiation resistance of the UHV GIS bushing is calculated by Equation (10), in which $h_1 = 8$ m, and $h_2 = 24$ m. The higher the frequency is, the greater the radiation resistance is, which means the higher radiation efficiency (Fig. 9). It is expected that the newly added radiation resistance will surely affect the high-frequency components of the VFTO.

The overhead busbar model has also been improved by taking into account the soil loss accurately. Located in the Yangtze River Basin, the low-frequency soil conductivity is relatively high, and the measured value is 0.03 S/m at 100 Hz. Due to the high conductivity of the soil, the dispersion effect mainly affects the real part of the earth impedance in the high frequency band.

For the other components of the test circuit, such as the basin insulator, CVT, power transformer, etc., the widely used models are adopted [34], [35], as shown in Table I.

C. Simulation Results

The VFTO calculation is performed by the proposed frequency domain algorithm. As the excitation source, the acting disconnector DS2 is modeled as the ideal step breakdown voltage source, with the internal resistance (i.e., the fixed arc resistance) of 4 Ω. The respective effects of radiation loss and soil loss are calculated and analyzed as follows.

Fig. 10 shows the effect of radiation loss of the GIS bushing, where the abscissas of the markers are the main frequencies extracted from the calculated VFTO spectrum, and the ordinates of the markers are the corresponding amplitudes. The frequency points of the first two maximum responses are 6.7 MHz and 200 kHz, which correspond to the main resonances of the GIS busbar and the overhead busbar, respectively. The radiation loss of the

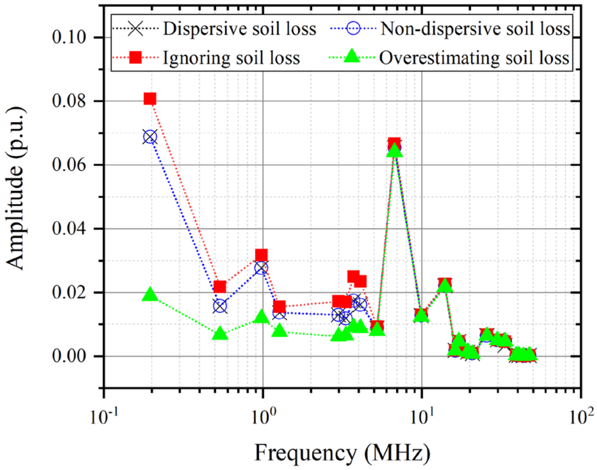

Fig. 11. Comparison between the amplitude–frequency responses of VFTO considering soil loss with dispersion, considering soil loss without dispersion, ignoring soil loss, and overestimating soil loss. The breakdown voltage used for calculation is 1 p.u.

GIS bushing has little effect on these two frequency points, but it presents a significant suppression effect on the high-frequency points such as 5.2, 14.0, 29.8, 33.4, and 47.4 MHz.

Fig. 11 shows the effect of soil loss along the overhead busbar. First, soil loss is considered in the simulation, which is divided into two cases: dispersive and non-dispersive, but there is almost no difference in the calculation results, indicating that the influence of soil dispersion on the VFTO calculation can be ignored. Second, the soil loss is not considered in the simulation, which will inevitably lead to an increase in the response. For example, the main frequency response of 200 kHz will increase by 17% if the soil loss is ignored. Third, the real part of the earth impedance is set to a fixed value for comparison. In our case, if the soil loss is approximated with the calculation at 30 MHz, it will result in lower low-frequency responses, such as a reduction at 200 kHz by 72%, which can be clearly seen in the figure. In short, soil loss with frequency-dependent characteristics should be considered, as it will affect the low-frequency response of VFTO.

D. Comparison of Simulation and Measurement

The calculated time-domain waveform is obtained by inverse Fourier transform of the VFTO spectrum, which has a sampling interval of 1 kHz and a total of 50 kS samples for the frequency band up to 50 MHz.

Fig. 12 compares the calculated and measured VFTO time-domain waveforms. The calculated waveform is offset based on the measured waveform, where the breakdown voltage is 1.2 p.u. and the source voltage is 0.4 p.u. at the arc breakdown. The comparison results are as follows.

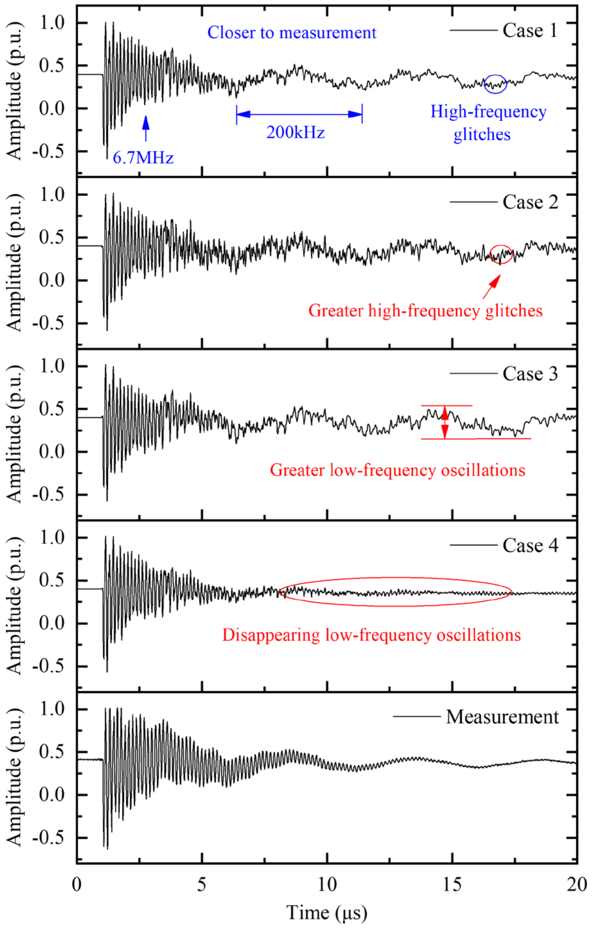

Fig. 12. Comparison of the calculated and measured VFTO waveforms at the end of the GIS branch busbar.(Case 1-4: Simulation results with different considerations of radiation loss and/or soil loss; Measurement: Waveform directly measured from the full-scale GIS test circuit.).

Case 1: When both the radiation loss and dispersive soil loss are considered, the calculated VFTO waveform has the best agreement with the measured waveform, with the high- and low-frequency oscillations clearly reflected. Evidently, the high- and low-frequency oscillations correspond to 6.7 MHz and 200 kHz, respectively.

Case 2: When only the soil loss is considered and the radiation loss is ignored, the calculated VFTO waveform has more evident higher-frequency “glitches”.

Case 3: When only the radiation loss is considered and the soil loss is ignored, the calculated VFTO waveform has higher oscillation amplitudes at 200 kHz.

Case 4: When the radiation loss is considered and the soil loss is overestimated, the low-frequency oscillation at 200 kHz almost disappears from the calculated VFTO waveform.

The difference between simulation and measurement is easier to draw from the response at the dominant frequencies, as shown in Table II. From the spectrum at 200 kHz, which is the main frequency point in the low-frequency band, the influence of soil loss is dominant, and the common overestimation of the soil loss in the time-domain algorithm has the highest impact on the calculation results. From the spectrum at frequency points exceeding 10 MHz, i.e., in the high-frequency band, the influence of radiation loss is dominant, and the calculated spectrum

TABLE II
SPECTRUM COMPARISON BETWEEN CALCULATED AND MEASURED WAVEFORMS AT REPRESENTATIVE FREQUENCY POINTS

Case No.	200 kHz	6.7 MHz	14.0 MHz	29.8 MHz	33.4 MHz	47.4 MHz
Case 1	0.069 +9.5%	0.067 -5.6%	0.022 -12%	0.0051 +13.3%	0.0043 +7.5%	0.00028 -9.7%
Case 2	0.069 +9.5%	0.067 -5.6%	0.034 **+36%**	0.0125 **+170%**	0.0075 **+87.5%**	0.00047 **+51.6%**
Case 3	0.081 **+28.6%**	0.067 -5.6%	0.023 -8%	0.0051 +13.3%	0.0045 +12.5%	0.00028 -9.7%
Case 4	0.019 **-69.8%**	0.064 -9.8%	0.022 -12%	0.0051 +13.3%	0.0046 +15%	0.00027 -12.9%
Measurement	0.063	0.071	0.025	0.0045	0.0040	0.00031

TABLE III
NOISE EVALUATED ON THE VFTO TIME-DOMAIN WAVEFORMS

Case No.	RMS Noise*	
	Evaluated by Mean Filter (10^{-5})	Evaluated by Median Filter (10^{-5})
Case 1	10.1361	7.1117
Case 2	56.0316	45.4088
Case 3	16.2456	9.4521
Case 4	7.0354	6.0155
Measurement	8.2069	5.3223

*To reduce the influence of the high-frequency components of the signal, the noises are evaluated at a time window from 10 μs to 20 μs.

deviates from the measured spectrum significantly when the radiation loss is not considered.

If regarding the glitches as a kind of additional white Gaussian noise (AWGN), they can be evaluated by mean power spectrum density. Since white noises are among the whole frequency band, smooth filters such as mean or median filters are adopted to evaluate the root mean square (RMS) noise and shown in Table III. It can be found that the Case 1 has the smallest glitches compared to the measurement if low-frequency oscillations are also required.

E. Discussion and Analysis

To sum up the results, we can now conclude that in the VFTO simulation considering the radiation loss of the GIS bushing helps to suppress the response of the high-frequency components, while considering the soil loss of the overhead busbar helps to improve the accuracy of the low-frequency amplitude.

From the perspective of insulation coordination, low-frequency oscillations influence the breakdown voltage of the GIS according to the v-t characteristic [36]. If the low-frequency oscillation of the VFTO is ignored, the risk of insulation breakdown will be underestimated in some cases. Therefore, a reasonable evaluation of the low-frequency oscillation intensity of the VFTO by considering the frequency-dependent characteristics of the earth impedance will help in the design of insulation coordination.

From the perspective of electromagnetic compatibility, at different frequencies, VFTO can conduct electromagnetic disturbances through instrument transformers with different transfer characteristics, or radiate electric fields to the surrounding environment with different emission efficiencies. Therefore, a reasonable evaluation of the high-frequency component of the VFTO by considering the radiation loss of the bushing can help evaluate the level of electromagnetic disturbance.

VI. CONCLUSION

In this study, GIS circuit models considering both the radiation and soil losses were developed, and their influences on the VFTO simulation were analyzed through a new frequency-domain algorithm. The models were then verified on the basis of measurements in a full-scale UHV GIS test circuit. It has been shown that the radiation loss expressed by the derived radiation resistance in the TL model of the GIS bushing plays an important role in suppressing the simulation response of the VFTO at frequencies above 10 MHz, making the high-frequency components much closer to the measured results. Although the effectiveness of frequency-dependent earth impedance is also confirmed in improving the accuracy within the low-frequency band, the influence of soil dispersion on the VFTO simulation can be neglected due to its small contribution to the low-frequency response of VFTO.

REFERENCES

[1] W. -J. Chen et al., “Study on the influence of disconnector characteristics on very fast transient overvoltages in 1100-kV gas-insulated switchgear,” *IEEE Trans. Power Del.*, vol. 30, no. 4, pp. 2037–2044, Aug. 2015.

[2] W. Chen et al., “Recent progress in investigations on very fast transient overvoltage in gas insulated switchgear,” *Proc. CSEE*, vol. 31, no. 31, pp. 1–11, 2011.

[3] Y. Li, Y. Shang, L. Zhang, R. Shi, and W. Shi, “Analysis of very fast transient overvoltages (VFTO) from onsite measurements on 800 kV GIS,” *IEEE Trans. Dielectrics Elect. Insul.*, vol. 19, no. 6, pp. 2102–2110, Dec. 2012.

[4] Z. Bajramovic et al., “Influence of substation’s elements on electromagnetic transient occurrences caused by disconnector switching,” *Electric Power Compon. Syst.*, vol. 39, no. 2, pp. 113–127, 2011.

[5] High-Voltage Switchgear and Controlgear—Part 203: Gas-Insulated Metal-Enclosed Switchgear for Rated Voltages Above 52 kV, IEC Standard 62271-203, Nov. 2003.

[6] S. Agematu et al., “High-frequency switching surge in substation and its effects on operation of digital relays in Japan,” in *Proc. CIGRE General Meeting*, Sep. 2006, pp. C4–304.

[7] A. Ametani et al., “Electromagnetic disturbances in gas-insulated substations and VFT calculations,” *Electric Power Syst. Res.*, vol. 160, pp. 191–198, 2018.

[8] J. A. Martinez, D. Povh, P. Chowdhuri, R. Iravani, and A. J. F. Keri, “Modeling guidelines for very fast transients in gas insulated substations,” Report Prepared by the Very Fast Transients Task Force of the IEEE Working Group on Modeling and Analysis of System Transients, Tech. Rep. PES-TR7 (TP133), pp. 6.1–6.24, 1998.

[9] H. W. Dommel and W. S. Meyer, “Computation of electromagnetic transients,” *Proc IEEE*, vol. 62, no. 7, pp. 983–993, Jul. 1974.

[10] J. Zhao, “Research on electromagnetic disturbances conducted by transformers and radiated from bushings in switch operations of UHV GIS disconnector,” Ph.D. dissertation, High Voltage Branch, China Electric Power Res. Inst., Jun. 2018.

[11] M. Rioual, “Measurements and computer simulation of fast transients through indoor and outdoor substations,” *IEEE Trans. Power Del.*, vol. 5, no. 1, pp. 117–123, Jan. 1990.

[12] D. Povh, H. Schmitt, O. Valcker, and R. Wutzmann, "Modeling and analysis guidelines for very fast transients," *IEEE Trans. Power Del.*, vol. 11, no. 4, pp. 2028–2035, Oct. 1996.

[13] T. Meng, X. Lin, and J. Xu, "Calculation of very fast transient over-voltage on the condition of segmental arcing model," *Trans. China Electrotechnical Soc.*, vol. 25, no. 9, pp. 69–73, 2010.

[14] S. A. Boggs, F. Y. Chu, N. Fujimoto, A. Krenicky, A. Plessl, and D. Schlicht, "Disconnect switch induced transients and trapped charge in gas-insulated substations," *IEEE Trans. Power App. Syst.*, vol. PAS-101, no. 10, pp. 3593–3602, Oct. 1982.

[15] F. M. Tesche, M. V. lanoz, and T. Karlsson, *EMC Analysis Methods and Computational Models*. Hoboken, NJ, USA: Wiley, 1997, pp. 250–266.

[16] K. C. Chen and K. M. Damrau, "Accuracy of approximate TL formulas for overhead wires," *IEEE Trans. Electromagn. Compat.*, vol. 31, no. 4, pp. 396–397, Nov. 1989.

[17] F. H. Silveira, S. Visacro, R. Alipio, and A. De Conti, "Lightning-induced voltages over lossy ground: The effect of frequency dependence of electrical parameters of soil," *IEEE Trans. Electromagn. Compat.*, vol. 56, no. 5, pp. 1129–1136, Oct. 2014.

[18] K. Sheshyekani and M. Akbari, "Evaluation of lightning-induced voltages on multiconductor overhead lines located above a lossy dispersive ground," *IEEE Trans. Power Del.*, vol. 29, no. 2, pp. 683–690, Apr. 2014.

[19] G. S. Lima and A. De Contib, "Bottom-up single-wire power line communication channel modeling considering dispersive soil characteristics," *Electric Power Syst. Res.*, vol. 165, pp. 35–44, 2018.

[20] Y. Baba and V. A. Rakov, "On the mechanism of attenuation of current waves propagating along a vertical perfectly conducting wire above ground: Application to lightning," *IEEE Trans. Electromagn. Compat.*, vol. 47, no. 3, pp. 521–532, Aug. 2005.

[21] H. Motoyama and H. Matsubara, "Analytical and experimental study on surge response of transmission tower," *IEEE Trans. Power Del.*, vol. 15, no. 2, pp. 812–819, Apr. 2000.

[22] H. Xue, A. Ametani, J. Mahseredjian, Y. Baba, F. Rachidi, and I. Kocar, "Transient responses of overhead cables due to mode transition in high frequencies," *IEEE Trans. Electromagn. Compat.*, vol. 60, no. 3, pp. 785–794, Jun. 2018.

[23] H. Xue, A. Ametani, and J. Mahseredjian, "Very fast transients in a 500 kV gas-insulated substation," *IEEE Trans. Power Del.*, vol. 34, no. 2, pp. 627–637, Apr. 2019.

[24] A. C. S. Lima and M. Y. Tomasevich, "Numerical issues in line models based on a thin wire above a lossy ground," *IEEE Trans. Electromagn. Compat.*, vol. 57, no. 3, pp. 555–564, Jun. 2015.

[25] T. A. Papadopoulos, G. K. Papagiannis, and D. P. Labridis, "A generalized model for the calculation of the impedances and admittances of overhead power lines above stratified earth," *Electric Power Syst. Res.*, vol. 80, pp. 1160–1170, 2010.

[26] E. D. Sunde, *Earth Conduction Effects in Transmission Systems*. New York, NY, USA: Van Nostrand, 1949.

[27] E. F. Vance, *Coupling to Shielded Cables*. Hoboken, NJ, USA: Wiley, 1978.

[28] D. Cavka, N. Mora, and F. Rachidi, "A comparison of frequency-dependent soil models: Application to the analysis of grounding systems," *IEEE Trans. Electromagn. Compat.*, vol. 56, no. 1, pp. 177–187, Feb. 2014.

[29] C. L. Longmire and K. S. Smith, "A universal impedance for soils," Defense Nuclear Agency, Santa Barbara, CA, USA, Topical Rep. Jul.–Sep. 1975.

[30] N. Nahman and D. Holt, "Transient analysis of coaxial cables using the skin effect approximation $A+$ *Bsqrts*," *IEEE Trans. Circuit Theory*, vol. 19, no. 5, pp. 443–451, Sep. 1972.

[31] F. Rachidi and S. Tkachenko, *Electromagnetic Field Interaction With Transmission Lines: From Classical Theory to HF Radiation Effects*. Southampton, U.K.: WIT Press, 2008.

[32] Y. Gongchang, L. Weidong, C. Weijiang, G. Yonggang, and L. Zhibing, "Development of full frequency bandwidth measurement of VFTO in UHV GIS," *IEEE Trans. Power Del.*, vol. 28, no. 4, pp. 2550–2557, Oct. 2013.

[33] W. Chen et al., "Experimental research on the characteristics of very fast transient overvoltage in ultra high voltage gas insulated switchgear," *Proc. CSEE*, vol. 31, no. 31, pp. 38–47, 2011.

[34] Z. Haznadar, S. Carsimamovic, and R. Mahmutcehajic, "More accurate modeling of gas insulated substation components in digital simulations of very fast electromagnetic transients," *IEEE Trans. Power Del.*, vol. 7, no. 1, pp. 434–441, Jan. 1992.

[35] D. Povh, H. Schmitt, O. Valcker, and R. Wutzmann, "Modelling and analysis guidelines for very fast transients," *IEEE Trans. Power Del.*, vol. 11, no. 4, pp. 2028–2035, Oct. 1996.

[36] G. Ueta, S. Kaneko, and S. Okabe, "Evaluation of breakdown characteristics of gas insulated switchgears for non-standard lightning impulse waveforms – breakdown characteristics under non-uniform electric field," *IEEE Trans. Dielectrics Elect. Insul.*, vol. 15, no. 5, pp. 1430–1438, Oct. 2008.

Jun Zhao was born in Jiangsu Province, China, in 1985. He received the B.S. degree in biomedical engineering and the M.S. degree in electrical machinery and appliances from the Huazhong University of Science and Technology, Wuhan, China, in 2007 and 2009, respectively, and the Ph.D. degree in high voltage and insulation technology from China Electric Power Research Institute, Beijing, China, in 2018. His research interests include electromagnetic transients due to switching operation and lightning in substations, and EMC immunity of secondary equipment in substations.

Weijiang Chen (Senior Member, IEEE) was born in Shandong Province, China, in 1958. He received the B.S. degree in electrical engineering from Hefei Industry University, Hefei, China, in 1982, and the M.S. degree in high voltage and insulation technology from China Electric Power Research Institute, Beijing, China, in 1985. From 2005 to 2008, he was the President of Wuhan High Voltage Research Institute, Wuhan, China. Since 2008, he has been the Vice Director of the UHV Department of State Grid Corporation of China. His research interests include over-voltage and insulation coordination of power system, gas discharge theory and application, and lightning protection. He was awarded the title of Academician of the Chinese Academy of Sciences in 2015.

Kejie Li was born in Shanxi Province, China, in 1989. He received the B.S. degree in electrical engineering and the Ph.D. degree in electrical engineering from Xi'an Jiaotong University, Xi'an, China, in 2012 and 2019, respectively. He is currently a Postdoctoral Researcher with the School of Electrical Engineering and Automation, Hefei University of Technology, Hefei, China. His research interests include modeling and analysis for electromagnetic transient, electromagnetic pulse generation, and electromagnetic susceptibility test and evaluation.

Kai Bian's photograph and biography is not available at the time of publication.

Jiangong Zhang's photograph and biography is not available at the time of publication.

Tao Wen's photograph and biography is not available at the time of publication.

Zihan Teng's photograph and biography is not available at the time of publication.